
Article:
Silverbush, D., Grosskurth, S., Wang, D. et al. (4 more authors) (2017) Cell-Specific Computational Modeling of the PIM Pathway in Acute Myeloid Leukemia. Cancer Research, 77 (4). pp. 827-838. ISSN 0008-5472

https://doi.org/10.1158/0008-5472.CAN-16-1578

Cell-Specific Computational Modeling of the PIM pathway in Acute Myeloid Leukemia

Dana Silverbush[1,2^], Shaun Grosskurth[3^], Dennis Wang[4], Francoise Powell[3], Bertie Gottgens[5], Jonathan Dry[3*] and Jasmin Fisher[2,6*]

[1]Department of Computer Science, Tel-Aviv University, Tel-Aviv, Israel;

[2]Microsoft Research, Cambridge, UK;

[3]AstraZeneca Oncology IMED, Waltham MA;

[4]AstraZeneca Oncology IMED, Cambridge UK;

[5]Department of Haematology, Cambridge Institute for Medical Research & Wellcome Trust and MRC Stem Cell Institute, University of Cambridge, UK;

[6]Department of Biochemistry, University of Cambridge, UK

^ These authors contributed equally to this work

*To whom correspondence should be addressed:

jf416@cam.ac.uk and jonathan.dry@astrazeneca.com

Running title: Cell-Specific Computational Models of Acute Myeloid Leukemia

Disclosure of Potential Conflicts of Interest: The authors have read and understood the AACR journal policy on reporting conflicts of interest and have no conflicts to disclose.

Abstract

Personalized therapy is a major goal of modern oncology, as patient responses vary greatly even within a histologically defined cancer subtype. This is especially true in acute myeloid leukemia (AML), which exhibits striking heterogeneity in molecular segmentation. When calibrated to cell-specific data, executable network models can reveal subtle differences in signaling that help explain differences in drug response. Furthermore, they can suggest drug combinations to increase efficacy and combat acquired resistance. Here we experimentally tested dynamic proteomic changes and phenotypic responses in diverse AML cell lines treated with pan-PIM kinase inhibitor and fms related tyrosine kinase 3 (FLT3) inhibitor as single agents and in combination. We constructed cell-specific executable models of the signaling axis, connecting genetic aberrations in FLT3, tyrosine kinase 2 (TYK2), platelet derived growth factor receptor alpha (PDGFRA), and fibroblast growth factor receptor 1 (FGFR1) to cell proliferation and apoptosis via the PIM and PI3K kinases. The models capture key differences in signaling that later enabled them to accurately predict the unique proteomic changes and phenotypic responses of each cell line. Furthermore, using cell-specific models, we tailored combination therapies to individual cell lines and successfully validated their efficacy experimentally. Specifically, we showed that cells mildly responsive to PIM inhibition exhibited increased sensitivity in combination with PIK3CA inhibition. We also used the model to infer the origin of PIM resistance engineered through prolonged drug treatment of MOLM16 cell lines and successfully validated experimentally our prediction that this resistance can be overcome with AKT1/2 inhibition.

Introduction

The potential of personalized medicine is dependent on our ability to translate the molecular context of patients' tumors into interpretable clinical outcomes. Successful steps have been taken to accurately predict tumor progression and response to treatment from molecular disease markers [1,2]. Using tumor cell line based compound screening, we can provide robust readouts of cellular responses to multiple compounds. This information can be used to systematically train computational models of the molecular signaling pathways contributing to drug sensitivity and resistance in various cancer settings, and to propose novel drug targets and combination approaches. Cell line screens have provided some success in explaining or predicting drug responses by driver gene mutations [2,3,4]; however in many cases the true mechanism of resistance remains elusive or more complex. Most predictive methods routinely used today employ correlative statistics or feature-based learning techniques such as machine learning, while network methods remain scarce despite their potential for extracting mechanistic insights and actionable biomarkers.

The molecular heterogeneity within cancer types further complicates the prediction of tumor cell behavior determining a patient's drug response. Multiple somatic mutations, epigenetic events or otherwise deregulated gene/protein expression may contribute to driving the disease. This is true in acute myeloid leukemia (AML), where patients may harbor somatic mutations in a number of potential oncogenes including FLT3, MLL, TYK2, FGFR1, PDGFRA, IDH1, DNMT3A, impacting expression of downstream signaling for example through PIM kinases [5,6,7]. FLT3 internal tandem duplications (FLT3-ITD) and PIM over-expression are associated with poor prognosis in AML patients, motivating the development of small molecule inhibitors targeting these proteins [8,9]. Incomplete signaling inhibition or the

presence of multiple molecular alterations that reduce a tumors dependency on any one target may result in drug resistance [10,11]. This may be overcome through rational drug combinations; however optimal approaches are rarely obvious and high throughput combination screening is complex and expensive with limited success shown.

With an aging population, the incidence of AML is increasing, with the number of new cases per year approaching 20,000 in the USA alone. AML therefore presents a large unmet clinical need, with overall 5-year survival rates remaining at around 25%. Most patients will respond to initial cytoreductive therapy but a large proportion will relapse with emergence of drug-resistant clones. Given that bone marrow transplantation as the only curative therapy is not an option for many patients, a better understanding of the regulatory pathways causing leukaemic transformation and in particular the emergence of resistance will be essential to improve treatment outcomes in AML.

Computational simulations of cancer cell signaling have the potential to overcome both the limitation of cell line diversity and *in-vitro* screening throughput. Computational modeling approaches can be used to capture and integrate knowledge with molecular and phenotypic data to better understand the genetic and signaling dependencies determining a drug's mechanism of action. The models should be unique to the tumor cell context, include key proteins and their interactions whilst accounting for influential gene mutations, and would ideally extend to other molecules involved in cell signaling. Execution of such models should demonstrate the intracellular signaling activity as it is triggered by different mutations and different therapeutic modalities, resulting in different cell phenotypes.

Computational models based around Boolean networks, pioneered by Kauffman [12] as a model for genetic regulatory networks, have been demonstrated for interpretation of large data sets as well as for drug discovery [13,14,15]. In these models, relationships are represented in a dynamic network with discrete time steps. Signaling molecules represented by nodes in a network can have two states (hence a Boolean network) and edges are directed and may be activating or inhibitory, however this can over-simplify biological signaling where molecules often exist in multiple states with interactions that are rarely binary. Qualitative Networks (QN) make an extension to Boolean networks to allow variables to range over larger discrete domains by replacing Boolean functions with algebraic functions [16] (further details in supplementary methods). Specifically the graphical tool Bio Model Analyzer (BMA) [17] (available at http://biomodelanalyzer.org/) has previously been used to encapsulate chronic myeloid leukemia (CML) cell signaling information from >150 publications in a QN model [18] able to then successfully recapitulate multiple independent experimental results. Another extention to Boolean networks is provided by Quantitative Modeling approaches, allowing variables to range over non-discrete values and so capturing more complex relationships, but only feasible for much smaller, well-studied systems [19].

In this study, we use QNs to model the protein signaling connecting genetic aberrations in FLT3, TYK2, PDGFRA or FGFR1 to cell proliferation/apoptosis via the PIM and PI3K kinases for four AML cell lines, accounting for their unique genetic and phenotypic diversity. Construction and analysis of the biological QN model was achieved in BMA [17]. By incorporating cell-specific context switches in the model for four cell lines, we were able to accurately model response and resistance to a pan-PIM kinase inhibitor AZD1208 and the FLT3 inhibitor AC220 and

validated experimentally our predictions. The model provides a useful tool for AML research, and the approach offers value to drug discovery and early development.

Materials and Methods

Reagents

AZD1208, AZD6244, and AZD5363 were synthesized by AstraZeneca R&D (Waltham, MA) and diluted in dimethyl sulfoxide (Sigma-Aldrich). AC220 and GDC0941 were purchased externally.

Cell line treatment

Cell lines (CMK, EOL1, HL60, KASUMI3, KG1A, MOLM13, MOLM16, MONOMAC6, MV411, NOMO1, OCIAML2, OCIM1, and OCIM2) were purchased from American Type Culture Collection (ATCC, http://www.atcc.org/) cell bank and passaged in our laboratory for fewer than 6 months after receipt or resuscitation. ATCC uses morphology, karyotyping, and PCR based approaches to confirm the identity of human cell lines and to rule out both intra- and interspecies contamination.

All cells were cultured and assayed as previously described in [8] and in supplemental methods.

Growth inhibition calculation

For single agent, GI_{50} were calculated from the ratio of the 72 hour treatment to 72 hour DMSO control, after subtraction of the Day 0 data from each measurement. The dose-response data were fitted using Xlfit (Microsoft Excel). For combination, percent growth inhibition was determined using the Chalice software with values of 0 to 100% indicating anti-proliferation (fewer number of cells than the vehicle control but greater than or equal to the number of cells at the start of treatment) and values of 101 to 200% indicating cell death (fewer cells than at the start of treatment). Day 0 values were subtracted from the Day 3 treatments. The combination Indexes (CI) and

Synergy scores were determined using the software program Chalice (Zalicus) and CI determination was made at the ED50 value. Synergy was determined by the Loewe additivity model.

Full methods for gene expression microarray; whole exome DNA sequencing; and Theranositcs proteomics are in the Supplemental Methods, brief description follows.

Gene expression microarray

Cell line lysate was generated from logarithmic growing CMK, EOL1, HL60, KASUMI3, KG1A, MOLM13, MOLM16, MONOMAC6, MV411, NOMO1, OCIAML2, OCIM1, and OCIM2 cell lines. Lysate was sent to Expression Analysis (http://www.expressionanalysis.com/) for gene expression analysis on Affymetrix Human Genome U133 Plus 2.0 Array. Expression results were fRMA normalized, log2 transformed, and expression was averaged by gene symbol across probesets.

Whole exome DNA sequencing

Cell lines lysate was generated from logarithmic growing CMK, EOL1, HL60, KASUMI3, KG1A, MOLM13, MOLM16, MONOMAC6, MV411, NOMO1, OCIAML2, OCIM1, and OCIM2. Lysate was sent to Expression Analysis (http://www.expressionanalysis.com/) for whole exome DNA sequencing, and processed with the BCBio pipeline (https://bcbio-nextgen.readthedocs.org). Paired analysis of the parental and resistant cell lines was performed to using FreeBayes [20], MuTect [21], and VarDict (GitHub) to call resistance specific mutations.

Theranostics Health reverse phased protein array

Cells were treated with AZD1208 or AC220 as single agent or in combination for 3 or 24 hours. Lysate was prepared and shipped to Theranostics Health (Rockville, Maryland) for reverse phased protein array experiments.

Protein Array data transformation for executable network model construction

The relative linear log2 RPPA values were categorized for use in executable network modelling (Fig S1) on a 5 point scale from 0-4 fitted to the distribution of the values (Table S1).

Protein western blots

Cells were treated with AZD1208, AZ5363, or AC220 as single agent, combination, or resistance as experimentally described. Whole cell extracts were fractionated by SDS-PAGE and transferred to a nitrocellulose membrane in transfer buffer (500mM Glycine, 50mM TrisHCl, 0.01% SDS, 10% methanol) buffer at 20Volts for 90 minutes using a semi-dry transfer apparatus according to the manufacturer's protocols (Invitrogen). The membranes are blocked with 10% nonfat milk in TBS-T (10 mM Tris, pH 8.0, 150 mM NaCl, 0.5% Tween 20) for 1 hour and washed three times with TBS-T and exposed to primary antibodies in 5% milk in TBS-T against pPRAS40 (CST 2997), p4EBP1 Ser 65 (CST 9451), pBAD (CST 9296), pp70S6 (CST 9206), pS6 (CST 4858), pERK (CST 9106), pelF4B (CST 8151), pAKT(CST 4058), α-tubulin (CST 2144) or β-actin (CST 4970) at 4 °C O/N. Membranes are washed three times for 10 minutes and incubated with a 1:10000 dilution of horseradish peroxidase-conjugated anti-mouse or anti-rabbit antibodies (CST 7074) for 1 hour at room temperature. After washing the membranes three times for ten minutes, signals were visualized using the ECL system (Thermo Scientific).

PhosphoScan mass-spectrometry

We confirmed the robusteness of our finding for MOLM16 cells treated with 2 uM AZD1208 for 3 hours (Table S2) by applying a LC-MS/MS phosphorylation proteomic approach. Additional details are provided in the Supplementary Note.

Targeted treatment of AML cell lines

We investigated phenotypic and cell signaling responses by reverse-phased protein arrays (RPPA). Since the PIM gene family is often over-expressed [22,23,24] and FLT3-ITD's are prevalent in AML [7], we treated the cells with the pan-PIM kinase inhibitor AZD1208 and the potent selective FLT3 inhibitor AC220 (Qizartinib) as monotherapy and in combination [25] and compared AML cell lines were treated with DMSO, 1uM AZD1208, 6nM AC220, or the respective combination, for 3 or 24 hours. Lysates were generated, protein values were assessed by RPPA and quadrant median normalized (QMN) protein levels calculated (Table S3). Statistically significant total protein and phosphorylation changes were determined by log2 QMN differences greater than or equal to 0.5 and Wilcoxon Rank Sum Tests p-values less than or equal to 0.1 (Table S4).

Results

AML cell lines show differential sensitivity to PIM inhibition

To identify potential genetic alterations associated with sensitivity to the pan-PIM kinase inhibitor AZD1208, we surveyed gene variants by whole exome DNA sequencing (Table S5) and prioritized by AML disease relevance [7]. Although cells sensitive to AZD1208 do harbor AML relevant PDGFRA, FGFR1, FLT3, and MLL genetic variants, only a small number of cell lines harbor the same variant, thereby failing to reach statistical significance in association to drug response (Fig 1A). Basal cell line *PIM1* mRNA expression tends to be higher in sensitive lines, as previously shown at the protein level [8], underlying the importance of compound target expression alongside the interplay with genetic alterations for sensitivity. However cells harboring pathway relevant genetic alterations or over-expressing PIM exhibit varied response to treatment, calling for a deeper examination of the cell signaling relating genotype to phenotype to provide a better understanding of the molecular dependencies underlying PIM inhibitor sensitivity in AML cell lines.

Cell type-specific differences in PIM pathway signaling in response to treatment

Given the wide variability of response to therapeutic agents across AML cell lines, we explored the differences in phospho-protein signaling downstream of PIM for AML cell lines MOLM16, MV411, EOL1 and KG1A. Reverse phase protein array (RPPA) measurements taken 24 hours post AZD1208 treatment reproduced published findings [8] of reduced BAD phosphorylation in the MOLM16 cell line, and reduced S6 pS235/236 in EOL1 (Fig 1B). To estimate response of cell lines, growth inhibition was quantified according to the number of viable cells after culturing with different concentrations of AZD1208 and FLT3 inhibitor, AC220, in combination (Fig 1C, Fig S2). Directional de-phosphorylation signaling trends seen in RPPA for BRAF pS445,

EIF4B pS406, MTOR pS2481 and global BAD phosphorylation were confirmed by PhosphoScan mass-spectrometry in MOLM16 cells after 3 hour treatment with AZD1208 (Table S6).

Building a generalized model of PIM signaling in AML

In order to model the observed genotypic and phenotypic differences between the AML cell lines, we proposed a workflow for developing a cell-specific context network model using the BMA tool from cell line molecular information (Fig 2). We generated an initial generalized model from the manual curation of 68 publications (Table S7) for AML cell line. The initial model contains a canonical set of 64 interactions among 32 interacting proteins connected to 2 cell phenotypes/behaviors of apoptosis and cell proliferation (http://www.bioc.cam.ac.uk/fisher/aml_-GeneralModel.json, Table S8). All values at nodes range from 0 to 4 to represent the phosphorylation activity from the transformed RPPA data, with 0 representing low to no activity and 4 representing abnormal over activity. The cellular behavior outcome for each disease state is reflected by the two terminal downstream nodes, which model the outcome for cellular abnormal proliferation and apoptosis rates. The generalized model of AML signaling was able to capture only partial abnormal cell behavior for untreated cells, capturing the abnormal low apoptosis levels for both MOLM16 and MV411, and showing an increase in proliferation, yet not capturing the magnitude of the increase. In addition, known perturbations such as simulating inhibition of PIMs in the model, showed the expected trend line of decreased proliferation, yet did not exhibit the expected effect on apoptosis levels.

Introducing cell-specific context in QN models

We incorporated multiple gene mutation switches (http://www.bioc.cam.ac.uk/fisher/aml - CellSpecificAML.json, Table 1) to construct cell-specific context model. We iteratively refined the target function for each internal node to reflect the levels of phosphorylation activity as measured by the transformed RPPA data for each cell line as well as the qualitative activity reported in the literature in accordance to gene mutations. A cell-specific context in the model is simulated by setting the switches for the driver mutations found in that cell to 1, while all other switches to mutations that were assessed as non-driver are set to 0 (Table S9). As a result of different set of mutations "turned on" the protein activity exhibited by the model will differ between cell lines (Table S10). Additional details on data processing and model construction are in the Supplementary notes.

Excutable QN model validated by cell type-specific signaling behaviour

The executable QN model (Fig 3A) was built on the RPPA and growth inhibition of MOLM16 and MV411 cell lines, harboring TYK2 mutation and FLT3-ITD respectively (Fig 1B). For each cell line across each treatment (Fig 3B), the mean square error (MSE) observed between the transformed RPPA values and modeled signaling activity ranged from 0.15 to 0.21 and median of 0.17 (0.3 to 0.57 in the generalized model, median of 0.41), with the lowest seen for MV411 cell line treated with AZD1208 + AC220 combination and the highest for the MOLM16 cell line treated with AZD1208. Meanwhile across each protein, the MSE observed between the transformed RPPA values and each protein signaling activity ranged from 0 to 0.36 and median of 0.29 (0.41 to 0.88 in the generalized model, median of 0.58), with the lowest seen for BAD and BCR and the highest seen for 4EBP1.

Equally as important, the cell-specific context model performed well in predicting cellular response as measured both by growth inhibition and markers of reduced proliferation and increased apoptosis (Fig 1B-C). The model accurately predicted (Fig 3C) the reduction in proliferation as a result of treatment with AZD1208 single agent, AC220 single agent, and drug combinations in MV411 cells. Although under predicting the magnitude of increase in apoptosis for AC220 single agent, the model accurately predicted the directional responses with increases in apoptosis for AZD1208 single agent, AC220 single agent, and combination treatments in MV411 cells.

In addition to predicting differential phenoptypic responses in each cell line, the model highlights key signaling events that may underlie the mechanism for each. We validated the robustness of events suggested for MOLM16 using mass-spectrometry. Most importantly, the mass-spectrometry corroborated the decreased EIF4B pS406 phosphorylation after AZD1208 treatment, contributing to decrease in proliferation, as well as the decrease in BAD pS112 and pS155 after AZD1208 treatment, which increases apoptosis. A key differentiating feature of MOLM16 cell lines is the lack of hyperactivity from the MAPK (Ras Raf MEK ERK) and AKT-mTORC1 pathways post AZD1208 treatment, supported by dephosphorylation at downstream BRAF pS445 and MTOR pS2481 in the mass-spectrometry data.

Testing the adaptability of the model to new cell-specific contexts, we "turned on" the genetic alterations FIP1L1-PDGFRA fusion and FGFR1 fusion, matching EOL1 and KG1A cell lines respectively. The apoptosis range was expanded to span the full dynamic range seen in these cell lines, yet no further refinement of the model was performed. The model reflected the cellular signaling changes observed in RPPA data (Fig 3D) where the MSE ranged from 0.18 to 0.28 with the lowest seen for EOL1 cell

line treated with single agent AZD1208 and the highest for the KG1A cell line treated in combination with AC220. Across each protein, the MSE observed between each protein signaling activity and the transformed RPPA values ranged from 0 to 0.58, with the lowest seen for AKT and the highest seen for p27. The model also performed well in predicting cellular response (Fig 3E). For the proliferation and apoptosis cell behaviors, the model accurately predicted the cellular responses seen in KG1A for AZD1208, AC220, and combination treatments, as well as the cell behaviors for EOL1 with AZD1208 treatment (AC220 was not tested for EOL1).

The model also replicated variations in sensitivity, such as EOL1 reacting with reduced apoptosis to PIM inhibition when compared to MOLM16.

Novel signaling components proposed through model refinement

A by-product of refining the QN model to capture cell type-specific signaling is a graphical and descriptive representation of cell specific signaling dynamics between proteins in the network (Fig 3A). By simulating the QN model, we were able to test our assumptions regarding the signaling dependencies between proteins, as described by the target functions (Table 1). For instance, despite FLT3-ITD being upstream of PIM1, the effect revealed by the iterative optimization of the model was less than other interacting proteins, also suggested by the RPPA measurements (Fig 1A) leading to BAD over-activity in MOLM16 but not MV411. The target function of AKT shows that it is dependent on the activity of the FLT3-ITD and FGFR1 fusion, reflecting the accumulation of evidences for AKT/mTOR pathway role in AML (suggested previously by [8]). The target function of S6 reflects the dominant over activation of it via AKT-mTOR pathway, additive to the activity of MAPK pathway, and leading to anti-apoptotic cell behavior of MV411 and KG1A. At the same time the target function of BAD accumulates with activity of MAPK pathway and of PIM1

direct phosphorylation of all three sites of BAD [26] leading to the anti-apoptotic behavior observed in MOLM16.

In silico virtual experimentation with AML cell models can replicate independently reported data

As a first independent test of the AML cell-specific model, we assessed its ability to replicate *in-silico* a sample of protein and phenotypic cell line responses to drug treatment reported in the literature but not used as part of model construction or refinement. We replicated each in-vitro experiment by turning on a respected set of mutations and adding the new examined inhibitor to the model, then observing the predicted protein expression. All eight protein changes were successfully predicted (Table S11). The model successfully predicted cell specific response to compounds including: failure of a MEK inhibitor to induce apoptosis in EOL1 [27]; insensitivity of KG1A to the combination of AKT, PDK1 and FLT3 inhibitors [28]; and the growth inhibition induced on EOL1 by combining PIM and AKT inhibition [11]. The decrease in cell proliferation of MV411 in response to mTORC [29] inhibitor was not recaptulated; however the authors of [29] attribute the decrease in proliferation to eIF4E decreased expression which was accurately replicated by the model.

AML cell-specific model predicts synergistic drug combinations with the PIM inhibitor

To assess the potential to prioritize synergistic combinations through *in silico* hypothesis testing with these models we assessed the PIM inhibitor AZD1208, the AKT inhibitor AZD5363, MEK inhibitor selumetinib (AZD6244, ARRY-142886), FLT3 inhibitor AC220, and PI3K inhibitor AZ2426 across the 4 AML cell lines (Fig 4A, Fig S3) also summarized in Table S12. For each cell line we simulated inhibiton of the drug targets first as single agents and then as combinations with PIM inhibition. We validated each combination in each cell line experimentaly across a dose range for each agent (Fig 4B).

The MOLM16 cell line was correctly predicted to be hyper-sensitive to the PIM inhibitor resulting in almost complete cell kill, and no additional effect was predicted in combination with other inhibitors.

In contrast, the MV411 context model, which habors a FLT3-ITD, correctly predicted a strong synergy between AZD1208 and AC220 combination attributed to apoptotic effect, evident even at lower dosage of combined treatments. Very weak synergy with mild apoptosis was correctly predicted in MV411 in combination with either MEK or PI3K inhibition.

Meanwhile, EOL1 was correctly predicted to gain apoptotic synergic effect with the PIM and AKT inhibitor combination, as well as the PIM and PI3K inhibitor combination. Surprisingly, and the only synergy of the 16 combinations not predicted by the model, EOL1 also exibited a synergic effect with the AZD1208 and AC220 combination. AC220 efficacy has previously only been reported in FLT3 driven tumors, however these data suggest efficacy from AC220 in PDGFRA mutated

tumors potetnially through inhibition of PDGFRA driven AKT/PI3K and MAPK signaling.

Finally, in the KG1A model, which harbors an activating FGFR1 fusion, we did not see a co-occurrence of high apoptosis and high growth inhibition for any of the combination treatments, validated as well by the *in-vitro* assays. Our model suggests that the persistant insensitivity of KG1A may be derived by the high levels of cMyc, which is not directly targeted by any of the combinations.

Executable QN model identify alternative susceptibilities in AZD1208 resistant cells

Four separate populations of MOLM16 cells were made resistant to PIM inhibition by growth in the presence of increasing doses of the compound over a four month period until resulting cell populations were able to maintain growth at 1uM AZD1208. While the parental MOLM16 cell has a 50nM GI50 in a 3 day MTS proliferation assay, all four resistant populations had GI50s greater than 9uM to AZD1208 over the same 3 day growth period (Fig S4A). RPPA measurements were taken for the parental and resistant cell lines.

We predicted candidate genetic causes of resistance by iteratively perturbing all individual and pairs of nodes in the parental MOLM16 model, and choosing those leading to similar signaling activity and phenotype as observed in the resistant populations, quantified by lower MSE (Fig S4B, S4C). This resulted in four different resistant contexts, one for each resistant cell population (Fig 5A). All contexts show over-activation through RAS/PI3K as well as AKT/MTOR signaling, supported by RPPA (Fig S4B). Interestingly, the different resistance contexts differ in their strength of altered signaling where resistant cell population R1 has a higher activity for both

pathways and resistant cell population R3 has lower activity for the AKT pathway. The predicted and observed pathway signaling suggests increased signaling activity through 4EBP1, EIF4B, S6, and BAD contributing to resistance. In particular it highlights AKT-S6 pathway as a major cause for the decreased apoptosis compared to MOLM16 parental when treated with AZD1208.

Whole exome DNA-seq was performed to identify potential protein altering genetic variants that could be driving the AZD1208 resistance. All variant calls with significant differences from the parental line (Table S13) were further parsed to highlight genes encoding proteins that have BIOGRID interactions (Table S14) to the RAS/PI3K and/or the AKT/MTOR signaling pathways (Fig 5B).

Using the four resistant MOLM16 context models, we predicted possible treatments to overcome resistance by simulating inhibition at each point through systematic addition of an inhibitor node to the network. In line with signalling changes, introduction of an AKT inhibitor AZD5363 to the resistant populations was predicted to overcome the AZD1208 resistance by blocking the abnormal PRAS40, 4EBP1 and S6 activity (Fig 5D). To test this prediction, parental MOLM16 and AZD1208 resistant populations were treated with and without 1uM AZD5363 for 1 hour. The resistant populations responded to AKT inhibition with AZD5363 by decreased pS235/235 S6 ribosomal protein and pT246 PRAS40 (Fig 5D), providing strong evidence for inhibition of AKT/MTOR signaling. The decrease in AKT/MTOR signaling was accompanied with an increase in cleaved PARP, indicating increased apoptosis and highlighting the dependency on this signaling pathway during AZD1208 resistance in MOLM16 cells.

Alternative qualitative modeling techniques

Qualitative models provide coarse-grained descriptions useful for systems whose mechanistic underpinnings remain incomplete. The range of qualitative modeling approaches provide two major types of simplifications: Boolean models relax the activity of biological entities to binary (ON or OFF), alternatively the relation of entities may be relaxed to simple logic operators (AND, OR, NOT). We explored the use of alternative approaches and robustness of findings by building a Boolean model and an AND/OR model via the same pipeline. For single agent PIM-inhibitor treatment the Boolean model was able to reasonably predict the proliferation and apoptotic responses in MOLM16 and KG1a, partially predicted proliferation response in EOL1, but poorly predicted responses in MV411 (Fig S5). The MV411 cell line was correctly predicted to response well to FLT3 inhibition. The model was not, however, able to predict treatment combination synergies (Fig S5). Since the Boolean model is simpler and easier to construct than a qualitative model it offers a useful tool for investigating single agent treatment in larger networks.

The AND/OR gated model recaptured most of the responses to single treatments, as well as synergistic combinations, revalidating the predictions made by our model (Fig S6). The synergistic response of KG1a to the combination of AZD1208 and AC220 was the only response not recaptured. This phenotype is likely derived by S6 additive activity from the MAPK pathway and AKT- mTORC1, which cannot be accurately described using AND/OR gates. AND/OR models may be generated by automated tools [30], and can serve well as an initial model scaffold. However more complex relationships such as those in our model between BAD, S6, 4EBP1, TSC2 and EIF4B in AML need to be further refined.

Discussion

The success of personalizing treatments for AML patients by tailoring to respective genetic alterations that characterize cancer subtypes has so far been limited. Moreover, drug responses seen in genetically matched patients or representative cell lines show considerable diversity [10,7]. By integrating both genomic and baseline proteomic data from AML cell lines with known tumor-driving genetic events we generated an AML network model capturing cell-context-specific signaling in the PIM kinase pathway. We developed a workflow methodology for constructing a network model with cell-specific context switches, which focuses on iterative refinement of the target function to reflect literature and experimental evidences. Users may also consider applying automated tools to decipher the target functions, such as CellNOpt-cFL tool developed by Morris et al. [30], and follow by manual refinement of the target functions.

The resulting cell-specific model captures cell specific signaling and response to cancer therapeutics, and provide virtual cell line models in which to test hypotheses for tailored therapy *in silico*. The cell-specific model significantly reduced the prediction error for both the baseline training data and on-treatment changes in protein expression compared to the generalized model. This is unsurprising since a generalized AML model insufficiently explains the heterogeneity in the mutational landscape and protein-signaling dynamics reported across different cell lines, for example a lack of signaling through AKT unique to cells with mutations in TYK2.

The cell-specific model accurately and directly recapitulated published experimental results for reported changes in expression in all 8 cases, and 9 out of 10 responses in cell behavior. These results are particularly remarkable when considering the potential

variability in signaling and phenotypic output over time, and the focus of these models on the cells steady state reflected by model stability.

We progressed to experimentally validate predictions made with the cell-specific model. The MV411 context model captured the signaling impact of the FLT3-ITD to correctly predict induction of apoptosis after treatment with PIM and PI3K inhibitors, and no effect with PI3K inhibitor alone [11]. For the cell line KG1A we identified contribution of high cMyc activity to cell proliferation, and correctly predicted insensitivity to inhibition of targets thought to be elevated by the FGFR fusion [28] including AKT, PDK1 and FLT3. The EOL1 context model identified previously unreported combination synergy between PIM and PI3KCA inhibitors, validated through increased tumor growth inhibition. This could lead to patients treated with lower doses of the inhibitors if the same efficacy is achieved by combinations, and thereby, reducing the risk of toxicity.

Model discrepancies highlight potential gaps in the captured network knowledge, and hypotheses that warrant further investigation. For example, our model fails to capture BCR and ERK overexpression following treatment in EOL1 and KG1a cell lines. This cannot be resolved through simple optimization of the current network, suggesting a potential gap in our knowledge of how the MAPK pathway influences these mechanisms (Fig 3D). We found that Siendones et al. [31] had also previously hypothesized the coexistence of transduction signal event, triggering the MAPK pathway independent of the FLT-ITD event, and coupled with poor response to FLT3 inhibitor. Investigating this discrepancy may shed new light on the resistance mechanism of these patients to FLT inhibitors.

Furthermore, using the MOLM16 context model we were able to systematically explore genetic changes that may render the cell resistant to PIM inhibition. Exome

sequencing and subsequent drug combination treatment of MOLM16 cell populations with acquired resistance to AZD1208 confirmed our predicted mechanistic dependency on AKT signaling and AKT inhibition as a second line therapy to overcome resistance.

By accurately predicting drug responses and combination synergies, and providing the mechanistic insight on the proteins driving the response, we highlight the ability of simulated models and virtual experimentation to prioritize effective therapies accompanied with associated predictive and dynamic biomarkers. Successful drug combinations could significantly augment therapy options for AML patients by overcoming innate and acquired resistance to drugs. Simulated qualitative models potentially offer a virtual platform to screen, discover and prioritize drug combinations *in silico*, focusing experimental approaches to validation. Comprehensive genetic diagnosis using targeted exome sequencing is already entering the clinic in major teaching hospitals. When coupled with emerging mass cytometry analysis (PMID: 26095251), all the biological information to build patient specific qualitative networks models may soon be available from frontline diagnostics data.

Taken together, the complexity of signaling pathways and the large number of resistance mechanisms mean that executable cellular models which are easily and quickly interpretable, like the ones we have presented here, are key for pinpointing potential combination therapies for different cancer types and subtypes. Furthermore, scaling these executable models to simulate patient-specific cancers paves the way for improved personalized treatments and enhanced precision medicine choices.

Acknowledgments

We would like to thank Dennis Huszar and Kirsten McEachern for their knowledge surrounding the PIM signaling network, Mika Ahdesmaki for performance of the DNA-seq alignment and variant calling, and Greg O'Connor for generation of the AZD1208 resistant MOLM16 cells. A central element of this study relied on single agents and combination cell line treatment; in particular we would like to thank Suping Wang and Erica Keaton for AZD1208 combination screen data, Keith Dillman for sample preparation and Western validation for FLT3 combinations & resistant cell lines; all from AstraZeneca. We would also like to thank Bloodwise for supporting BG, and the Israeli ministry of science, technology and space and Edmond J. Safra Center for Bioinformatics at Tel-Aviv University for supporting DS.

References

[1] B Majumder, U Baraneedharan, S Thiyagarajan, P Radhakrishnan, H Narasimhan, M Dhandapani, N Brijwani, D D Pinto, A Prasath, B U Shanthappa, A Thayakumar, R Surendran, G K Babu, A M Shenoy, M A Kuriakose, G Bergth, P Horowitz , "Predicting clinical response to anticancer drugs using an ex vivo platform that captures tumour heterogeneity," *Nature Communications*, vol. 6, p. ncomms7169, 2015.

[2] JC Costello,LM Heiser,E Georgii,M Gönen,MP Menden,NJ Wang,M Bansal,M Ammad-ud-din,P Hintsanen,SA Khan,JP Mpindi,O Kallioniemi,A Honkela,T Aittokallio,K Wennerberg,NCI DREAM Community,J Collins,D Gallahan,D Sing,JS Rodriguez,S KaKaski,JW Gray,G Stolovitzky , "A community effort to assess and improve drug sensitivity prediction algorithms," *Nature biotechnology*, pp. 32(12):1202-12., 2014.

[3] P Geeleher, NJ Cox, RS Huang. , "Clinical drug response can be predicted using baseline gene expression levels and in vitro drug sensitivity in cell lines.," *Genome Biology*, pp. 15(3):R47., 2014.

[4] B Yadav, T Pemovska, A Szwajda, E Kulesskiy, M Kontro, R Karjalainen, MM Majumder, D Malani, A Murumägi, J Knowles, K Porkka, C Heckman, O Kallioniemi, K Wennerberg, T Aittokallio. , "Quantitative scoring of differential drug sensitivity for individually optimized anticancer therapies.," *Scientific Reports*, pp. 4:5193., 2014.

[5] G Marcucci, T Haferlach, H Döhner. , "Molecular genetics of adult acute myeloid leukemia: prognostic and therapeutic implications.," *Journal of clinical oncology*, pp. 29(5):475-86., 2011.

[6] H Wang, H Hu, Q Zhang, Y Yang, Y Li, Y Hu, X Ruan, Y Yang, Z Zhang, C Shu, J Yan, EK Wakeland, Q Li, S Hu, X Fang. , "Dynamic transcriptomes of human myeloid leukemia cells.," *Genomics.*, pp. 102(4):250-6., 2013.

[7] Cancer Genome Atlas Research Network TCGA, "Genomic and epigenomic landscapes of adult de novo acute myeloid leukemia.," *The New England journal of medicine*, pp. 30;368(22):2059-74, 2013.

[8] EK Keeton, K McEachern, KS Dillman, S Palakurthi, Y Cao, MR Grondine, S Kaur, S Wang, Y Chen, A Wu, M Shen, FD Gibbons, ML Lamb, X Zheng, RM Stone, DJ Deangelo, LC Platanias, LA Dakin, H Chen, PD Lyne, D Huszar. , "AZD1208, a potent and selective pan-Pim kinase inhibitor, demonstrates efficacy in preclinical models of acute myeloid leukemia.," *Blood*, pp. 123(6):905-13, 2014.

[9] KM Kampa-Schittenhelm, MC Heinrich, F Akmut, H Döhner, K Döhner, MM Schittenhelm. , "Quizartinib (AC220) is a potent second generation class III tyrosine kinase inhibitor that displays a distinct inhibition profile against mutant-FLT3, -PDGFRA and -KIT isoforms.," *Mol Cancer.*, pp. 12:19., 2013.

[10] JM Klco, DH Spencer, CA Miller, M Griffith, TL Lamprecht, M O'Laughlin, C Fronick, V Magrini, RT Demeter, RS Fulton, WC Eades, DC Link, TA Graubert, MJ Walter, ER Mardis, JF Dipersio, RK Wilson, TJ Ley. , "Functional heterogeneity of genetically defined subclones in acute myeloid leukemia.," *Cancer Cell.*, pp. 25(3):379-92., 2014.

[11] K Meja, C Stengel, R Sellar, D Huszar, BR Davies, RE Gale, DC Linch, A Khwaja. , "PIM and AKT kinase inhibitors show synergistic cytotoxicity in acute myeloid leukaemia that is associated with convergence on mTOR and MCL1

pathways.," *British journal of haematology*, pp. 167(1):69-79., 2014.

[12] S Kauffman, "Homeostasis and Differentiation in Random Genetic Control Networks," *Nature*, pp. 177-178, 1969.

[13] S Kauffman, "Metabolic stability and epigenesis in randomly constructed genetic nets," *Journal of Theoretical Biology*, pp. 437-467, 1969.

[14] S Huang, "Gene expression profiling, genetic networks, and cellular states: an integrating concept for tumorigenesis and drug discovery," *Journal of molecular medicine*, pp. 469-480, 1999.

[15] L Sanchez, D Thieffry. , "A logical analysis of the Drosophila gap-gene system," *Journal of theoretical biology*, pp. 115-141, 2001.

[16] MA Schaub, TA Henzinger, J Fisher. , "Qualitative networks: a symbolic approach to analyze biological signaling networks," *BMC Systems Biology*, p. 4+, 2007.

[17] D Benque, S Bourton, C Cockerton, B Cook, J Fisher, S Ishtiaq, N Piterman, A Taylor, M Y Vardi , "Bma: Visual Tool for Modeling and Analyzing Biological Networks," *Computer Aided Verification (CAV)*, pp. 686–692, 2012.

[18] Benjamin A. Hall, David Benque, Byron Cook, Samin Ishtiaq, Nir Piterman, Alex Taylor, Moshe Vardi, Steffen Koschmieder, Berthold Gottgens & Jasmin Fisher Ryan Chuang, "Drug Target Optimization in Chronic Myeloid Leukemia Using Innovative Computational Platform," *Scientific Reports*, vol. 5, February 2015.

[19] Assieh Saadatpour and Réka Albert, "A comparative study of qualitative and quantitative dynamic models of biological regulatory networks," *EPJ Nonlinear Biomedical Physics*, June 2016.

[20] E Garrison, G Marth. , "Haplotype-based variant detection from short-read sequencing.," *arXiv preprint arXiv*, p. 1207.3907, 2012.

[21] K Cibulskis, MS Lawrence, SL Carter, A Sivachenko, D Jaffe, C Sougnez, S Gabriel, M Meyerson, ES Lander, G Getz. , "Sensitive detection of somatic point mutations in impure and heterogeneous cancer samples.," *Nature biotechnology*, pp. 31(3):213-9., 2013.

[22] R Amson, F Sigaux, S Przedborski, G Flandrin, D Givol, A Telerman , "The human protooncogene product p33pim is expressed during fetal hematopoiesis and in diverse leukemias.," *Proceedings of the National Academy of Sciences of the United States of America*, pp. 86(22):8857-61, 1989.

[23] J Asano, A Nakano, A Oda, H Amou, M Hiasa, K Takeuchi, H Miki, S Nakamura, T Harada, S Fujii, K Kagawa, I Endo, K Yata, A Sakai, S Ozaki, T Matsumoto, M Abe , "The serine/threonine kinase Pim-2 is a novel anti-apoptotic mediator in myeloma cells.," *Leukemia*, pp. 25(7):1182-8, 2011.

[24] M Mizuki, J Schwable, C Steur, C Choudhary, S Agrawal, B Sargin, B Steffen, I Matsumura, Y Kanakura, FD Böhmer, C Müller-Tidow, WE Berdel, H Serve. , "Suppression of myeloid transcription factors and induction of STAT response genes by AML-specific Flt3 mutations," *Blood*, pp. 101(8):3164-73, 2003.

[25] PP Zarrinkar, RN Gunawardane, MD Cramer, MF Gardner, D Brigham, B Belli, MW Karaman, KW Pratz, G Pallares, Q Chao, KG Sprankle, HK Patel, M Levis, RC Armstrong, J James, SS Bhagwat. , "AC220 is a uniquely potent and selective inhibitor of FLT3 for the treatment of acute myeloid leukemia (AML).," *Blood*, pp. 114(14):2984-92, 2009.

[26] LL Yuan, AS Green, S Bertoli, F Grimal, V Mansat-De Mas, C Dozier, J

Tamburini, C Récher, C Didier, S Manenti. , "Pim kinases phosphorylate Chk1 and regulate its functions in acute myeloid leukemia.," *Leukemia.*, pp. 28(2):293-301., 2014.

[27] C Nishioka, T Ikezoe, J Yang, A Yokoyama. , "Inhibition of MEK/ERK signaling induces apoptosis of acute myelogenous leukemia cells via inhibition of eukaryotic initiation factor 4E-binding protein 1 and down-regulation of Mcl-1.," *Apoptosis.*, pp. 15(7):795-804., 2010.

[28] Z Zeng, IJ Samudio, W Zhang, Z Estrov, H Pelicano, D Harris, O Frolova, N Hail, W Chen, SM Kornblau, P Huang, Y Lu, GB Mills, M Andreeff, M Konopleva , "Simultaneous inhibition of PDK1/AKT and Fms-like tyrosine kinase 3 signaling by a small-molecule KP372-1 induces mitochondrial dysfunction and apoptosis in acute myelogenous leukemia," *Cancer Research*, pp. 3737-3746, 2006.

[29] L Willems, N Chapuis, A Puissant, TT Maciel, AS Green, N Jacque, C Vignon, S Park, S Guichard, O Herault, A Fricot, O Hermine, IC Moura, Auberger P, N Ifrah, F Dreyfus, D Bonnet, C Lacombe, P Mayeux, D Bouscary, J Tamburini , "The dual mTORC1 and mTORC2 inhibitor AZD8055 has anti-tumor activity in acute myeloid leukemia," *Leukemia*, pp. 1195–1202, 2012.

[30] J Saez-Rodriguez, D C. Clarke, P K. Sorger, D A. Lauffenburger M K. Morris, "Training Signaling Pathway Maps to Biochemical Data with Constrained Fuzzy Logic: Quantitative Analysis of Liver Cell Responses to Inflammatory Stimuli," *PLoS computational biology*, March 2011.

[31] N. Barbarroja, L. A. Torres, P. Buendía, F. Velasco, G. Dorado, A. Torres, and C. López-Pedrera E. Siendones, "Inhibition of Flt3-activating mutations does not prevent constitutive activation of ERK/Akt/STAT pathways in some AML cells:

a possible cause for the limited effectiveness of monotherapy with small-molecule inhibitors.," *Hematological oncology*, vol. 25, pp. 30-37, March 2007.

Table 1. Target functions for AML cell specific calibrated AML model. Target functions are associated to the nodes and aim to capture biological relationships. MAX function corresponds to independent activation by upstream proteins, while MIN corresponds to dependent activation, such that the effect is governed by the lower expression of the two upstream proteins. + corresponds to an additive effect, and * is used to assign magnitude of effect. Table S1 extends this table and includes the Generalized Model and experimental and literature supporting evidences for each target function.

Protein/Node	Cell-Specific Model Target Function
PIM1	max(3/4*FltITD,TYK2,3/4*PDGFRA,FGFR1)
PIM2	max(FltITD,1/2*TYK2,1/2*PDGFRA)
BAD	1/2*RSK+1/2*PIM1
EIF4B	min(3,RSK+1/2*PIM1)
EIF3	min(EIF4E,EIF4B)
4EBP1	2/3*mTORC1+1/6*EIF3+1/6*PIM2
EIF4E	max(1/2*4EBP1,S6)
S6	1/8*RSK+3/4*mTORC1+1/8*EIF3
BCR	max(1, 1/2*FltITD)
Grb2/SOS	max(BCR,1/2*FGFR1)
RAS	min(Grb2/SOS,BCR)
PI3K	max(BCR,Grb2/SOS,1/2*PDGFRA)
RAF	AVG(RAS)
MEK	AVG(RAF)
ERK	max(MEK,1/2*PDGFRA)
RSK	AVG(ERK)
AKT	max(PI3K,mTORC2)
mTORC2	AVG(PI3K)
mTORC1	1/2*PRAS40+TSC2
TSC2	1/2*((PIM2-1)+1/2*Akt)
PRAS40	1/4*PIM1+5/4*Akt
CHK	max(PIM1,PIM2)
H3	AVG(CHK)
cMyc	max(3/4*FGFR1,max(1,1/4*(max(PIM1,PIM2) + H3))
P27	max(1,var(cMyc)*(var(cMyc)-
Proliferation	(EIF4B-2)+1/2*ERK+2/3*p27+2/3*cMyc

Apoptosis	!MAX(BAD, S6, 1/2*BAD + cMyc + S6 + 2*EIF4E))

Figure 1. AML cell lines sensitive to the PIM inhibitor AZD1208 have diverse genotypes. (A) GI50 (uM) waterfall plot and molecular oncoprint illustrating the diverse pharmacological response of AML cells after 72 hours AZD1208 treatment as well as PIM expression and AML disease relevant mutations. Boxed cell lines names indicate responding cell lines further investigated. **(B)** Protein expression measured by reverse-phase protein array (RPPA) in treated and untreated cell lines show heterogeneity in signaling responses through various pathways. **(C)** MV411, with an active FLT3-ITD, shows varied responses to concentrations of AZD1208 and/or AC220 for 72 hours. The number of viable cells was determined by Alamar Blue measurements where the values represent percent growth inhibition.

Figure 2. Schematic workflow of cell-specific model construction in BMA. Motifs and interactions curated from the literature are used to build a Qualitative Network in the BMA tool. The model was calibrated with the results of RPPA experiments for two cell lines with different AML-driving mutations. The model is designed to represent the general AML pathways, and provide a cell-specific context by "turning-on" a specific set of mutations. The mutations impact outgoing interactions, thus activating the pathways in a mutation-specific manner, resulting in mutation-specific phosphorylation activity throughout the pathways leading to specific cellular behavior. The model is iteratively refined by testing and comparing to the cell behavior measured as a response to different perturbations for the two cell lines. The model robustness was tested against perturbations from the literature performed on the explored mutations, and unseen cell lines incorporated automatically into the model. The model is then used for *in-silico* experimentation in order to test novel drug combinations, infer the source and mechanism for drug resistance, and predict drug response in resistant cell lines and suggest treatment for resistance.

Figure 3. Generation of a predictive cell behavior model for AML training cell lines (MOLM16 and MV411) and unseen cell lines (EOL1 and KG1A) (A) Cell-Specific AML regulatory network model incorporating knowledge from the literature and calibrated to phosphorylation activity measured by RPPA. Perturbations, driving mutations, and internal genes are depicted in grey, green, and red, respectively. To simulate specific cell (MOLM16, MV411, EOL1 or KG1A) the node for the protein with driver mutations (TYK2, FLT-ITD, PDGFRA, or FGFR1 respectively) is set to 1, while all other proteins with mutations are set to 0. **(B)** Protein signaling activity (phosphorylation) levels inferred *in-silico* using the cell-specific contexts (laptop icon), and the generalized model (papers icon) capturing levels of phosphorylation activity as measured *in-vitro* (petri-dish). **(C)** Cell apoptosis and proliferation as inferred *in-silico* by the executable model compared to levels as observed *in-vitro*, with the generalized model capturing partial abnormal cell behavior, and the cell-specific context model recapitulating measured levels. **(D)** Unseen cell lines EOL1 and KG1A are incorporated to the executable network model. The robustness of the model is tested via the ability of the model to capture the phosphorylation activity unseen at the time of model construction, and **(E)** Cell behavior as a result of different perturbations**.**

Figure 4. Validation of predicted synergistic combinations of drugs reveals new effective treatment strategies. (A) Cell-Specific AML model is used to test combinations of drugs and predict cell behavior in a cell specific manner. A drug or a combination of drugs is simulated by partially or fully nullifying the target functions of their targets, and can be done automatically and efficiently with a large number of candidates. **(B)** Predicted cell behavior of apoptosis and proliferations is validated via growth inhibition of AML cell lines cultured with the indicated concentration ranges of AZD1208 and/or tested combined inhibitor after 72 hours. Predicted synergic effect, as seen for EOL1 cell line with PIM and AKT and PIM and PI3K inhibitors, is used to prioritize combinations.

Figure 5. Origin of resistance to AZD1208 in MOLM16 is computationally inferred and validated via whole exome DNA-seq, revealing signaling mechanism validated via western blots and offers combination to combat resistance which successfully induces apoptosis. (A) Network model of MOLM16 resistant cell populations (R1-4). Perturbations (lightning bolts) were automatically predicted at specific nodes to simulate possible resistance mechanisms that would attenuate signaling down a specific pathway (shaded red and blue). **(B)** Whole exome DNA-seq was performed on the 1uM AZD1208 resistant pool population to identify protein altering variants from variant calling as significantly different from the parental MOLM16 cell line. Genes whose proteins are involved with epigenetic machinery are underlined with dashes. **(C)** Inferred signaling activity from the parental MOLM16 executable model is compared to activity from western blots for parental and resistant cell populations. **(D)** Predictions of signaling activity and cell apoptosis for AZD1208 treated alone and in combination with AKT inhibitor AZD5363 is compared to activity from western blots. Prediction of induced apoptosis is supported by the increase in PARP Cleaved with AZD5363.

Figure 1

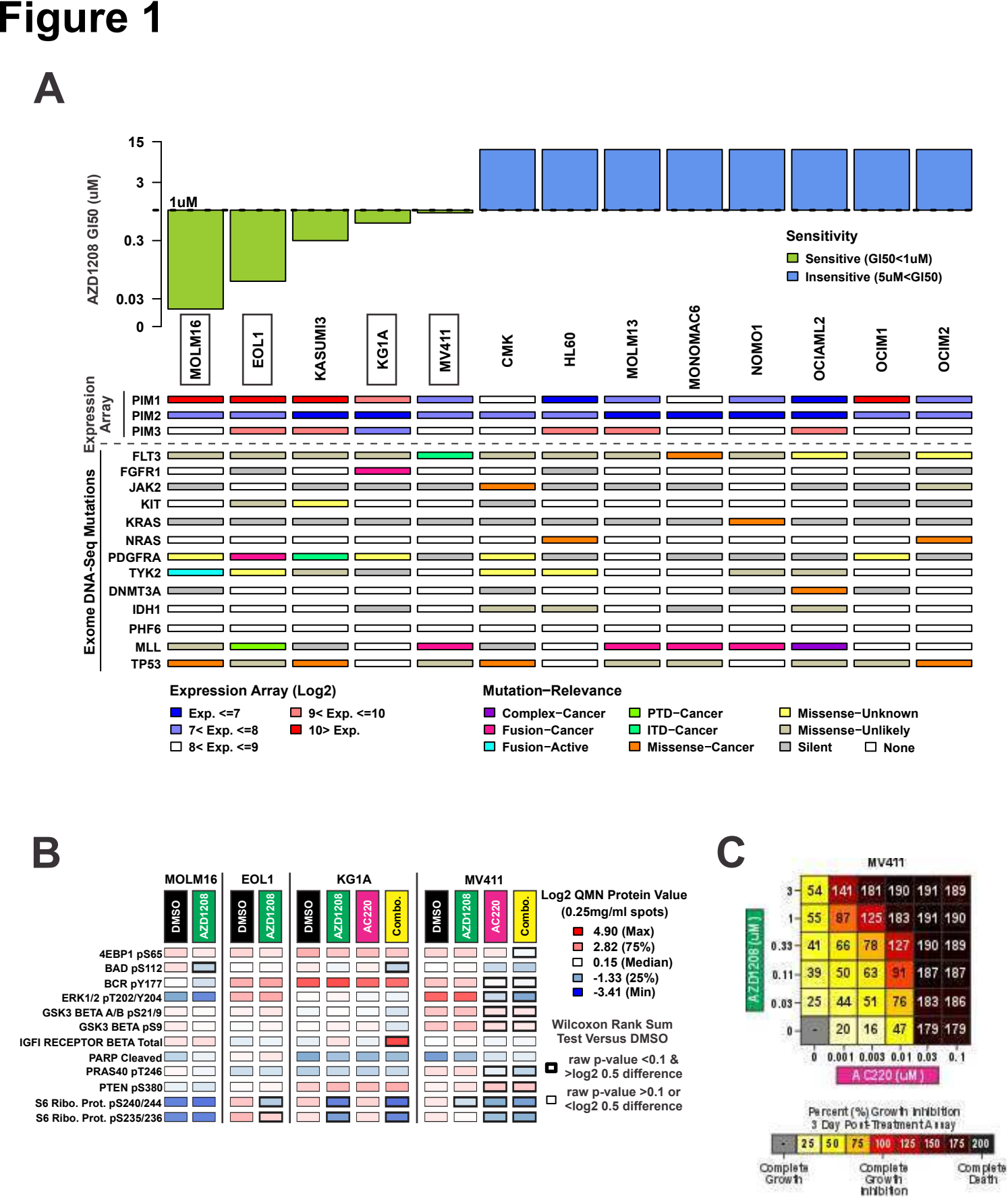
A
AZD1208 GI50 (uM)
15
3
0.3
0.03
0
1uM
Sensitivity
Sensitive (GI50<1uM)
Insensitive (5uM<GI50)
MOLM16
EOL1
KASUMI3
KG1A
MV411
CMK
HL60
MOLM13
MONOMAC6
NOMO1
OCIAML2
OCIM1
OCIM2
Expression Array
PIM1
PIM2
PIM3
Exome DNA-Seq Mutations
FLT3
FGFR1
JAK2
KIT
KRAS
NRAS
PDGFRA
TYK2
DNMT3A
IDH1
PHF6
MLL
TP53
Expression Array (Log2)
Exp. <=7
7< Exp. <=8
8< Exp. <=9
9< Exp. <=10
10> Exp.
Mutation−Relevance
Complex−Cancer
Fusion−Cancer
Fusion−Active
PTD−Cancer
ITD−Cancer
Missense−Cancer
Missense−Unknown
Missense−Unlikely
Silent
None
B
MOLM16
EOL1
KG1A
MV411
DMSO
AZD1208
AC220
Combo.
4EBP1 pS65
BAD pS112
BCR pY177
ERK1/2 pT202/Y204
GSK3 BETA A/B pS21/9
GSK3 BETA pS9
IGFI RECEPTOR BETA Total
PARP Cleaved
PRAS40 pT246
PTEN pS380
S6 Ribo. Prot. pS240/244
S6 Ribo. Prot. pS235/236
Log2 QMN Protein Value
(0.25mg/ml spots)
4.90 (Max)
2.82 (75%)
0.15 (Median)
-1.33 (25%)
-3.41 (Min)
Wilcoxon Rank Sum
Test Versus DMSO
raw p-value <0.1 &
>log2 0.5 difference
raw p-value >0.1 or
<log2 0.5 difference
C
MV411
AZD1208 (uM)
3 54 141 181 190 191 189
1 55 87 125 183 191 190
0.33 41 66 78 127 190 189
0.11 39 50 63 91 187 187
0.03 25 44 51 76 183 186
0 - 20 16 47 179 179
0 0.001 0.003 0.01 0.03 0.1
AC220 (uM)
Percent (%) Growth Inhibition
3 Day Post-Treatment Assay
- 25 50 75 100 125 150 175 200
Complete Growth
Complete Growth Inhibition
Complete Death

Figure 2

Model Construction

RPPA

	AML Cell 1		AML Cell 2	
Treatment	1	2	1	2
Protein 1 pS				
Protein 1 pT				
Protein 2 pT				
Protein 2 Total				
Protein ... pS				
Protien ... pT				
Protein ... Total				

Literature

Driver Mutantions

Signaling

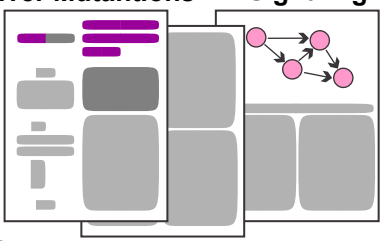

BMA AML Model

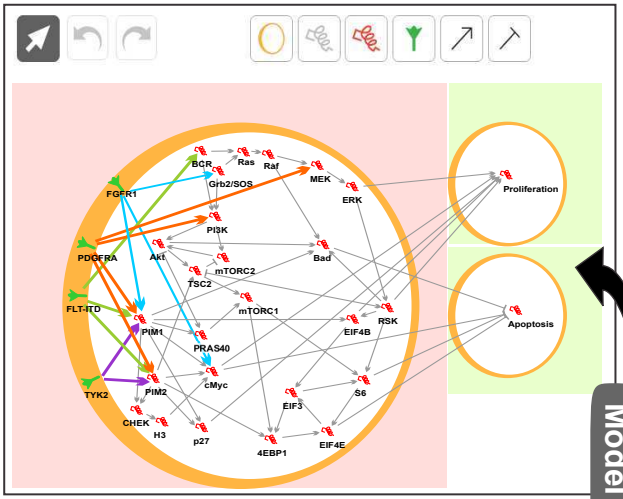

Model Refinement

Model Validation

1. Cell Behavior

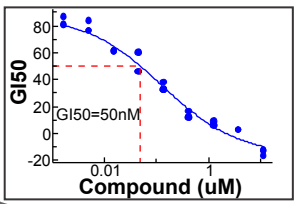

2. Perturbations from Literature

Paper	Cell Line	Drug	Results	Inferred
3	MOLM16	PIM Inhibition	PRAS40 neglectalby effected	PRAS40 (2 -› 1)
			4EBP1 neglectalby effected	4EBP1 (2 -› 1)
			S6 slightly more	S6 (2 -› 1)
			Significant effect on apoptosis	apoptosis increased (0 -› 3)

3. Additional Cell Lines

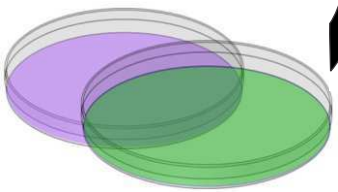

In Silico Experimentation

1. New Drug Combinations
2. Mechanisms for Drug Resistance

Prediction Validation

1. Combinations Increased Sensitivity
2. Drug Tailored to Resistant Mechanism Initiated Apoptosis

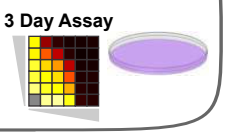

Figure 3

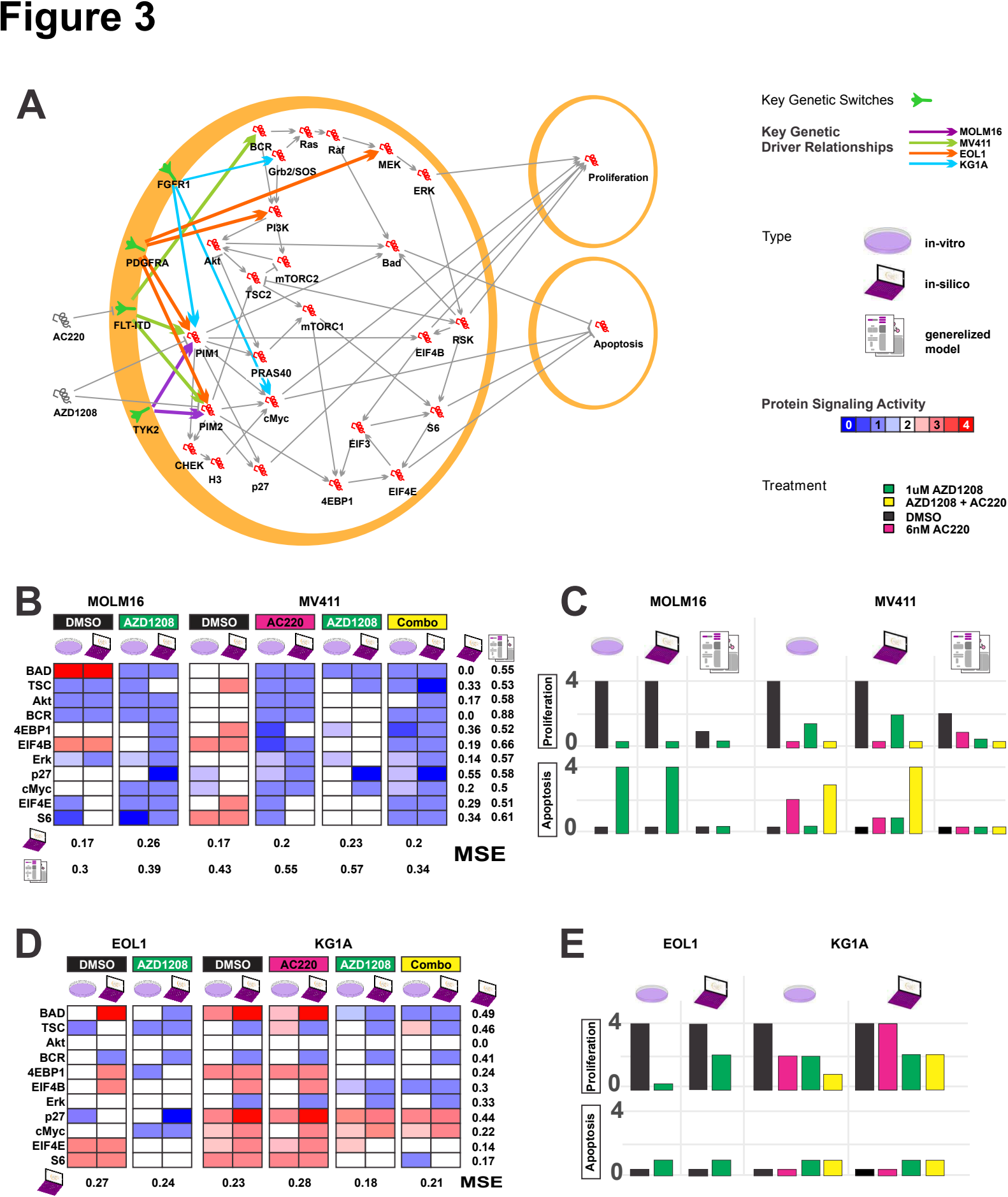
A
Key Genetic Switches
Key Genetic Driver Relationships
MOLM16
MV411
EOL1
KG1A
Type
in-vitro
in-silico
generelized model
Protein Signaling Activity
0 1 2 3 4
Treatment
1uM AZD1208
AZD1208 + AC220
DMSO
6nM AC220
BCR
Ras
Raf
MEK
ERK
Grb2/SOS
FGFR1
PI3K
PDGFRA
Akt
Bad
mTORC2
TSC2
mTORC1
RSK
EIF4B
Proliferation
Apoptosis
AC220
FLT-ITD
PIM1
PRAS40
AZD1208
TYK2
PIM2
cMyc
S6
EIF3
CHEK
H3
p27
4EBP1
EIF4E
B
MOLM16
MV411
DMSO
AZD1208
DMSO
AC220
AZD1208
Combo
BAD
TSC
Akt
BCR
4EBP1
EIF4B
Erk
p27
cMyc
EIF4E
S6
0.0 0.55
0.33 0.53
0.17 0.58
0.0 0.88
0.36 0.52
0.19 0.66
0.14 0.57
0.55 0.58
0.2 0.5
0.29 0.51
0.34 0.61
0.17 0.26 0.17 0.2 0.23 0.2
0.3 0.39 0.43 0.55 0.57 0.34
MSE
C
MOLM16
MV411
Proliferation
Apoptosis
4
0
D
EOL1
KG1A
DMSO
AZD1208
DMSO
AC220
AZD1208
Combo
BAD
TSC
Akt
BCR
4EBP1
EIF4B
Erk
p27
cMyc
EIF4E
S6
0.49
0.46
0.0
0.41
0.24
0.3
0.33
0.44
0.22
0.14
0.17
0.27 0.24 0.23 0.28 0.18 0.21
MSE
E
EOL1
KG1A
Proliferation
Apoptosis
4
0

Figure 4

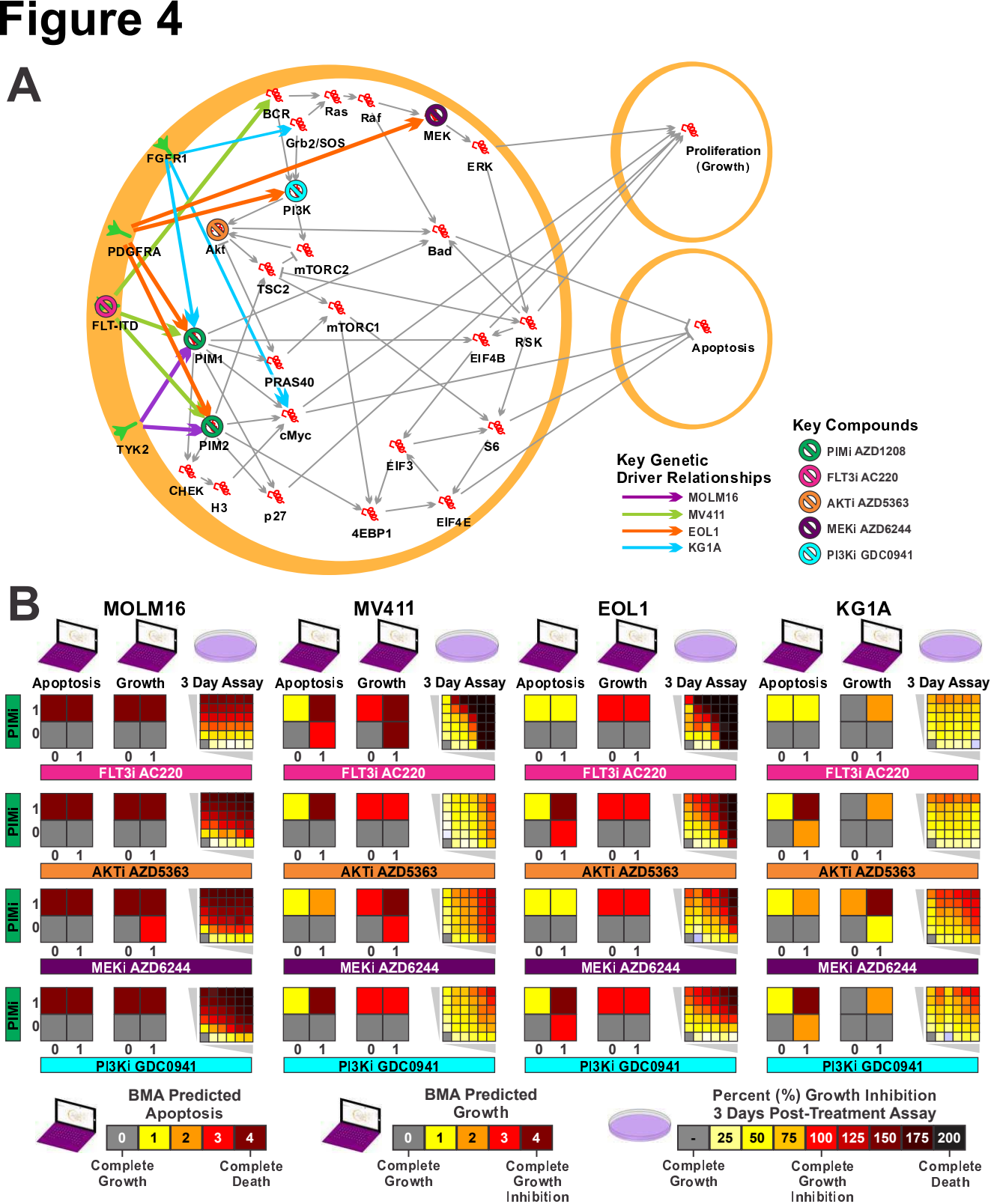
A
BCR
Ras
Raf
MEK
ERK
Grb2/SOS
FGFR1
PI3K
PDGFRA
Akt
Bad
mTORC2
TSC2
FLT-ITD
mTORC1
PIM1
RSK
EIF4B
PRAS40
cMyc
TYK2
PIM2
S6
EIF3
CHEK
H3
p27
4EBP1
EIF4E
Proliferation (Growth)
Apoptosis
Key Genetic Driver Relationships
MOLM16
MV411
EOL1
KG1A
Key Compounds
PIMi AZD1208
FLT3i AC220
AKTi AZD5363
MEKi AZD6244
PI3Ki GDC0941
B
MOLM16
MV411
EOL1
KG1A
Apoptosis
Growth
3 Day Assay
PIMi
FLT3i AC220
AKTi AZD5363
MEKi AZD6244
PI3Ki GDC0941
BMA Predicted Apoptosis
0 1 2 3 4
Complete Growth
Complete Death
BMA Predicted Growth
0 1 2 3 4
Complete Growth
Complete Growth Inhibition
Percent (%) Growth Inhibition 3 Days Post-Treatment Assay
- 25 50 75 100 125 150 175 200
Complete Growth
Complete Growth Inhibition
Complete Death

Figure 5

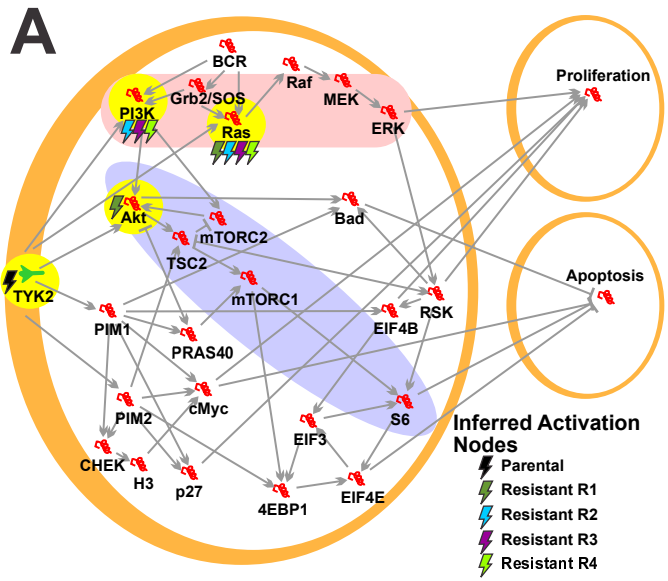
A
BCR
Raf
MEK
ERK
Grb2/SOS
PI3K
Ras
Proliferation
Akt
Bad
mTORC2
TSC2
Apoptosis
TYK2
mTORC1
RSK
PIM1
EIF4B
PRAS40
cMyc
PIM2
S6
EIF3
CHEK
H3
p27
4EBP1
EIF4E
Inferred Activation Nodes
Parental
Resistant R1
Resistant R2
Resistant R3
Resistant R4

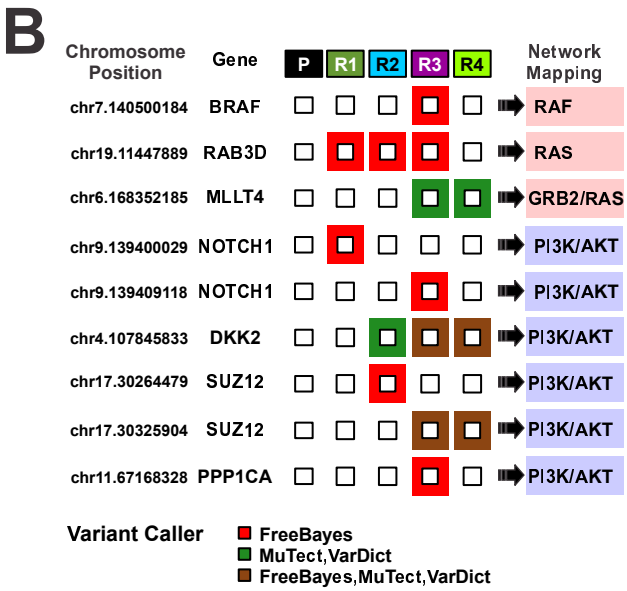
B
Chromosome Position
Gene
P
R1
R2
R3
R4
Network Mapping
chr7.140500184 BRAF RAF
chr19.11447889 RAB3D RAS
chr6.168352185 MLLT4 GRB2/RAS
chr9.139400029 NOTCH1 PI3K/AKT
chr9.139409118 NOTCH1 PI3K/AKT
chr4.107845833 DKK2 PI3K/AKT
chr17.30264479 SUZ12 PI3K/AKT
chr17.30325904 SUZ12 PI3K/AKT
chr11.67168328 PPP1CA PI3K/AKT
Variant Caller
FreeBayes
MuTect,VarDict
FreeBayes,MuTect,VarDict

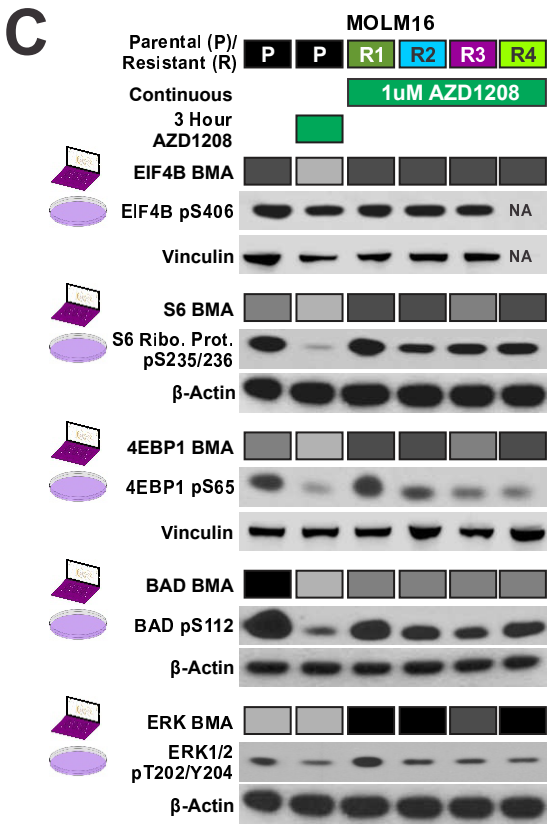
C
MOLM16
Parental (P)/ Resistant (R)
P
P
R1
R2
R3
R4
Continuous
1uM AZD1208
3 Hour AZD1208
EIF4B BMA
EIF4B pS406
NA
Vinculin
NA
S6 BMA
S6 Ribo. Prot. pS235/236
β-Actin
4EBP1 BMA
4EBP1 pS65
Vinculin
BAD BMA
BAD pS112
β-Actin
ERK BMA
ERK1/2 pT202/Y204
β-Actin

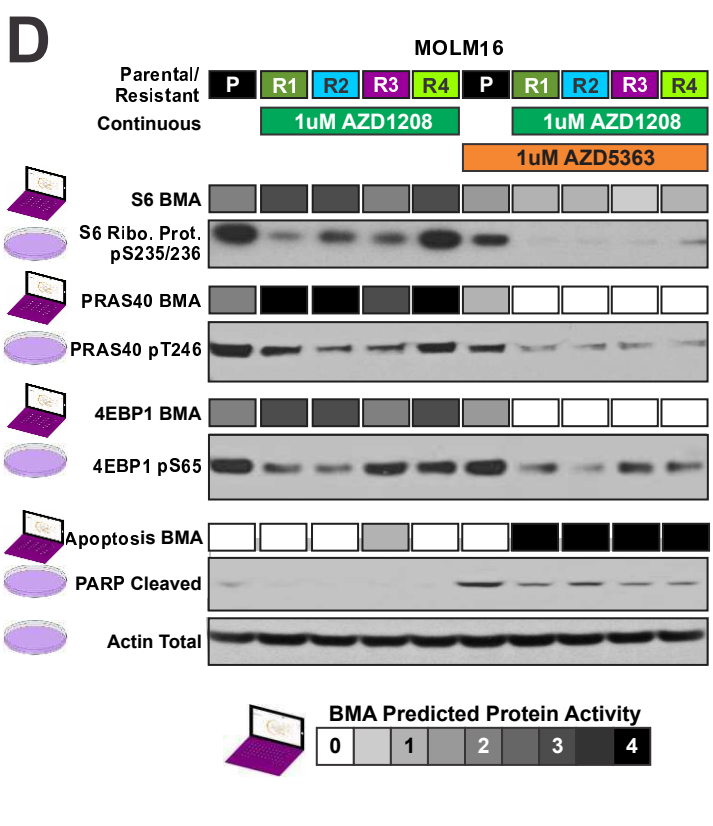
D
MOLM16
Parental/ Resistant
P
R1
R2
R3
R4
P
R1
R2
R3
R4
Continuous
1uM AZD1208
1uM AZD1208
1uM AZD5363
S6 BMA
S6 Ribo. Prot. pS235/236
PRAS40 BMA
PRAS40 pT246
4EBP1 BMA
4EBP1 pS65
Apoptosis BMA
PARP Cleaved
Actin Total
BMA Predicted Protein Activity
0
1
2
3
4